Stem Cell Research (2013) 11, 938–950

Available online at www.sciencedirect.com

SciVerse ScienceDirect

www.elsevier.com/locate/scr

Loss of androgen receptor promotes adipogenesis but suppresses osteogenesis in bone marrow stromal cells

Chiung-Kuei Huang[a], Kuo-Pao Lai[a], Jie Luo[a], Meng-Yin Tsai[b], Hong-Yo Kang[b], Yuhchyau Chen[c], Soo Ok Lee[a,*], Chawnshang Chang[a,d,**]

[a] George Whipple Lab for Cancer Research, Departments of Pathology, Radiation Oncology, Urology, and The Wilmot Cancer Center University of Rochester Medical Center, Rochester, NY 14642, USA
[b] Center for Menopause and Reproductive Medicine Research, Chang Gung University and Hospital, Kaohsiung, Taiwan
[c] Department of Radiation Oncology, University of Rochester Medical Center, Rochester, NY 14642, USA
[d] Sex Hormone Research Center, China Medical University and Hospital, Taichung 404, Taiwan

Received 11 March 2013; received in revised form 29 May 2013; accepted 2 June 2013
Available online 10 June 2013

Abstract Gender differences have been described in osteoporosis with females having a higher risk of osteoporosis than males. The differentiation of bone marrow stromal cells (BMSCs) into bone or fat is a critical step for osteoporosis. Here we demonstrated that loss of the androgen receptor (AR) in BMSCs suppressed osteogenesis but promoted adipogenesis. The mechanism dissection studies revealed that AR deficiency suppressed osteogenesis-related genes to inhibit osteoblast differentiation from BMSCs. Knockout of AR promoted adipogenesis of BMSCs via Akt activation through IGFBP3-mediated IGF signaling, and the 5′ promoter assay and chromatin immunoprecipitation assays further proved that AR could modulate IGFBP3 expression at the transcriptional level. Finally, addition of IGF inhibitors successfully masked the AR deficiency-induced Akt activation, and inhibitions of Akt, IGF1, and IGF2 pathways reversed the AR depletion effects on the adipogenesis process. These results suggested that AR-mediated changes in IGFBP3 might modulate the IGF–Akt axis to regulate adipogenesis in BMSCs.

Introduction

Gender differences have been described in osteoporosis with the female gender having higher risk of osteoporosis and fracture than the male gender (Boling, 2001; Khosla et al., 1999). The lineage differentiation balance between bone and fat in bone marrow stromal cells (BMSCs) is a critical determinant in development of osteoporosis (Rosen and Bouxsein, 2006). Previous studies have shown that postmenopausal women have a higher risk of osteoporosis than men

* Correspondence to: S.O. Lee, George Whipple Lab for Cancer Research, Departments of Pathology, Radiation Oncology, Urology, and The Wilmot Cancer Center University of Rochester Medical Center, Rochester, NY 14642, USA
** Correspondence to: C. Chang, Sex Hormone Research Center, China Medical University and Hospital, Taichung 404, Taiwan.
E-mail addresses: soook_lee@urmc.rochester.edu (S.O. Lee), chang@urmc.rochester.edu (C. Chang).

1873-5061/$ - see front matter © 2013 Elsevier B.V. All rights reserved.
http://dx.doi.org/10.1016/j.scr.2013.06.001

at similar ages and that estrogen administration alleviates osteoporosis in postmenopausal women, suggesting that the fluctuation of estrogen levels is critical in bone absorption and resorption (Lufkin et al., 1992). Similar phenotypes in obesity were also observed in postmenopausal women as the estrogen declined, indicating that estrogen affects adipocyte differentiation (Carney, 2010; Freeman et al., 2010; Ryan et al., 2002). However, estrogen levels cannot account for the gender differences in male, since bone and fat in male are mainly influenced by androgen (Alibhai et al., 2012; Cilotti and Falchetti, 2009; Galvao et al., 2008; Keto et al., 2012).

Clinical observations, from prostate cancer patients treated with androgen deprivation therapy, have pointed out that androgen/AR signaling is involved in osteoporosis and obesity. The observations suggested that androgen enhances osteogenesis and suppresses adipogenesis (Collier et al., 2011). To better understand the AR function in osteogenesis and adipogenesis, Kawano et al. and Yeh et al. generated androgen receptor knockout (ARKO) mice and clearly demonstrated that AR deficiency leads to osteoporosis and increases obesity due to increased osteoclast activity in bone and abnormal metabolism in white adipose tissues (Kawano et al., 2003; Yeh et al., 2002). In addition, Balkan et al. directly treated MC3T3-E1, an osteoblast progenitor cell line, with androgen and concluded that androgen could stimulate osteoblast differentiation (Balkan et al., 2005). Kang et al. used ARKO mice to prove AR deficiency leads to tissue-nonspecific alkaline phosphatase down-regulation followed by decreased phosphate production to cause reduced bone mineralization (Kang et al., 2008). Similar results were obtained from the osteoblast specific ARKO mouse showing that AR could stimulate osteoblast differentiation and attenuate bone resorption (Chiang et al., 2009; Notini et al., 2007). Recently, Tsai et al. showed that ARKO mouse displayed osteoporosis with decreased osteogenesis of BMSCs through down-regulation of Runx2/Cbfa1 (Tsai et al., 2011). In our study, we used the microarray assay to systematically analyze ARKO effects on osteogenesis related genes and found AR plays a promoter role in osteogenesis.

While AR effects on adipogenesis of BMSCs remain elusive, using microarray analysis we found that the genes in bone related categories, such as skeletal system development, ossification, bone development, and osteoblast differentiation, were down-regulated when AR was knocked out in primary BMSCs, whereas the genes in the adipose related category were not significantly altered in AR knocked out BMSCs. With the molecular mechanism dissection, we found AR increases insulin-like growth factor binding protein 3 (IGFBP3) through direct binding to its promoter region. The IGFBP3 modulated by AR might then participate in inhibiting Akt activation to cause less adipocyte differentiation.

Materials and methods

Cells, animals and reagents

Oil Red O and alizarin red powders were purchased from Sigma Aldrich. Dihydrotestosterone (DHT) ELISA kit was purchased from Enzo Life Science. Mlu I and Kpn I were purchased from New England BioLabs. IGFBP3, AR, and GAPDH antibodies were from Santa Cruz Biotechnology. Akt, pAkt, ERK1/2, pERK1/2, JNK, and pJNK were purchased from Cell Signaling Technology. Floxed AR/AR female mice were established as we described in our previous publication (Yeh et al., 2002). The EIIa $Cre^{+/+}$ mice were purchased from Jackson Lab. To establish wild type (WT) and ARKO mice, the floxed AR/AR female mice were bred with EIIa $Cre^{+/+}$ mice to obtain the floxed $AR^{+/y}$ Ella $Cre^{+/-}$ as ARKO mice and the $AR^{+/y}$ Ella $Cre^{+/-}$ as WT control. The primers used for genotyping were as described previously (Huang et al., 2012). All animal studies followed the "Guide for the Care and Use of Laboratory Animals" (National Institutes of Health publication). The protocols were reviewed and approved by the University Committee on Animal Resources of University of Rochester.

Bone microcomputed tomography and histomorphometry

12 weeks old WT and ARKO mice were euthanized with an overdose of pentobarbital. The bones from the hind limbs were taken out and cleaned with a scalpel to remove muscles and connective tissues. The bone microcomputed tomography and histomorphometry were performed and analyzed as previously described (Kang et al., 2008).

Fertility test

The fertility test was performed as previously described (Xu et al., 2007). Basically, 3 WT and ARKO male mice were bred with 2 proven fertile female mice. Male mice were kept for 10 days with 2 female mice and then female mice were removed to other cages for 28 days to determine whether they were pregnant. Pregnancy was assessed by the generation of litters during that 28-day period. Fertility results were expressed as average pup numbers/litter.

Hematoxylin and eosin staining

Adipose tissues were dehydrated and embedded into paraffin blocks. 5 tissue slides were prepared for hematoxylin and eosin (H&E) staining. Briefly, tissue slides were deparaffined, rehydrated, and stained with H&E as previously described (Lai et al., 2012). After staining, tissue slides were dehydrated and mounted with mounting medium. Images were taken with Spot software using Nikon Camera and analyzed with Image Pro Plus.

Detection of DHT

Mice at 8 weeks old were euthanized and blood collected using cardiac puncture (Lai et al., 2009). Sera were isolated using the blood collection tubes by centrifuging the samples for 30 min. 50 μl of sera was used to determine the DHT levels following the instruction manual from Enzo Life Science.

Colony forming efficiency assay

Primary BMSCs were isolated from 8 weeks old mice following the established method (Bianco et al., 2006). Colony forming efficiency assays were performed following previous publications with some modifications (Castro-Malaspina et al., 1980; Sacchetti et al., 2007). 2×10^5 mononucleated cells per well were seeded onto 6-well plates. After culture for 21 days, cells were fixed with methanol and washed with ddH_2O. Cells were stained with 1% methylene blue for 15 min and rinsed with ddH_2O twice. Images were taken with Nikon Camera. Image Pro Plus was used to analyze the number of CFU-*f* positive colonies (>50 cells).

Culture of human BMSCs

Human BMSCs were purchased from Millipore and maintained with human BMSC expansion medium following the instruction manual. Cultured human BMSCs were analyzed within 10 passages.

Microarray analysis

WT and ARKO BMSCs were isolated and cultured from 8 weeks old male mice (Bianco et al., 2006). The hematopoietic lineage cells were depleted with the magnetic bead isolation protocol as we previously described (Lee et al., 2012). The kit was purchased from Miltenyi Biotec (Auburn, CA). Briefly, 10^7 bone marrow cells were resuspended in 40 μl PBS buffer containing 2 mM EDTA and 0.5% BSA. 10 μl biotin-antibody cocktails containing antibodies for hematopoietic lineage were mixed with resuspended cells and incubated for 20 min on ice. 30 μl buffer and 20 μl anti-biotin microbeads were incubated with samples for 20 min on ice. After incubation, the samples were put into DynaMag™-2 Magnet (Invitrogen) for 2 min and the bound beads were moved to each side. At this step, cells not bound to beads were taken out and cultured for experiments. The confluent cultured BMSCs were lysed to extract mRNA, and 10 μg fresh mRNA used to determine the whole gene changes via mouse affymetrix microarray. The assay and analysis procedures were as previously described (Faith et al., 2008). The gene category was classified using DAVID bioinformatics resources as previously described (Huang da et al., 2009).

Differentiation assay

Adipogenesis

BMSCs were seeded onto 6-well plates and cultured until reaching confluence. The confluent cells were induced with adipogenic media (DMEM + 10% FBS + 2 μg/ml Insulin + 1 μM dexamethasone + 2 μM Rosiglitazone) for 6 days. Human BMSCs were induced to differentiate into adipocytes using the same differentiation media. The adipocytes containing oil droplets were visualized with Oil Red O staining (Yu et al., 2008).

Osteogenesis

BMSCs were seeded onto 6-well plates and cultured until reaching confluence. The confluent cells were induced with osteogenic media (DMEM + 10% FBS + 50 μg/ml ascorbic acid + 10 mM β-glycerophosphate). Human BMSCs were differentiated into osteocytes with the same osteogenic media. The mineralized osteocytes were visualized with alizarin red staining.

Lentivirus infection

HEK-293T cells were used to produce lentivirus by calcium-phosphate transfection. 12 μg lentivirus plasmid (pLVTHM-scramble, pLVTHM-AR-siRNA, pWPI, pWPI-AR), 8 μg pCMVdeltaR8.91 containing GAG and POL, and 10 μg pMD2.G containing VSVg) were used to produce virus in 60 mm^2 dishes. The human siRNA-AR used in this study was prepared as previously described (Chuang et al., 2009). Culture media containing virus were collected 40 h after transfection and filtrated through 0.45 μm filter to remove cell debris or cells. The collected virus media were used to infect cells in the presence of polybrene (2 μg/ml) for 24 h. Media containing virus were removed, fresh media were added to infected cells, and the cells were cultured for another 3 days to allow target protein expression. Since the lentiviral vectors express green fluorescence protein (GFP), fluorescence microscopy was used to monitor the infection efficiency via checking the GFP signal.

Western blot analysis assay

Cell lysates were resolved with 10% sodium dodecyl sulfate-polyacrylamide gel electrophoresis (SDS-PAGE), blotted with antibodies mentioned before, and incubated with correlated secondary antibodies conjugated with horseradish peroxidase. Proteins were visualized according to the manual instructions (Pierce ECL Western Blotting Substrate, Thermo Scientific). Tubulin or GAPDH served as loading control. The quantitation results were calculated using Quantitative ONE software (Bio-Rad) and expressed as relative value to loading control.

RNA extraction and real time quantitative PCR (qRT-PCR)

Total RNAs were extracted with Trizol (Invitrogen) according to the manufacturer's instructions. One μg mRNAs were used to be reverse transcribed to cDNAs using Superscript III (Invitrogen). Quantitative qRT-PCR was performed using cDNA, specific gene primers, and SYBR green master mix (BioRad) on an iCycler iQ Multi-color real-time PCR machine (BioRad). qRT-PCR results were calculated as relative expressions to the control and normalized to the housekeeping gene, GAPDH. All primers used for qRT-PCR were summarized in Supplemental Table 2.

Plasmid construction

The pGL3-IGFBP3-luciferase was constructed by ligating pGL3-luciferase and IGFBP3 promoter region. The IGFBP3 promoter was cloned out using primers as described in Supplemental Table 3. Both PCR product and pGL3-Luciferase vector were digested with Kpn I and Mlu I restriction enzymes.

The digested products were ligated with T4 ligase overnight at 16 °C and then transformed with DH5α. Transformed DH5α were grown on the ampicillin selection agar to select out positive clones that contain IGFBP3 promoter region hooked with pGL3-luciferase.

Chromatin immunoprecipitation assay

Cultured WT and ARKO BMSCs were treated with 37% formaldehyde to crosslink chromatin with proteins and 1 M glycine was used to stop the reaction. Cells were washed three times with PBS containing a cocktail of proteinase inhibitors. Pellets were lysed with SDS lysis buffer and sonicated as previously described (Kang et al., 2008). The sonicated samples were pre-cleared with protein agarose A/G and salmon sperm, diluted with ChIP dilution buffer, and incubated with either IgG control or AR antibody overnight. The samples were incubated with protein A/G-agarose to pull down the chromatin complex. The pellets were washed with low salt buffer, high salt buffer, immunocomplex wash buffer, and TE buffer. The chromatins were eluted out from the complex with elution buffer. The crosslinked chromatins were reversed with NaCl and the products were examined using DNA purification and PCR assay. The primers used for PCR were as described in Supplemental Table 3. The PCR product length of androgen response element (ARE) 2 is 279.

Statistical analysis

Values were expressed as mean ± standard deviation (S.D.). The Student's *t* test was used to calculate *p* values. *p* values were two-sided, and considered statistically significant when <0.05.

Results

ARKO mice show osteoporosis and obesity

In order to clarify the AR role in osteoporosis and obesity, we generated ARKO mice by mating floxed AR/AR female mice with male mice expressing EIIa cre recombinase (Coumoul et al., 2005), driven by the adenoviral *EIIa* promoter. Genotyping data clearly showed both WT and ARKO mice expressed cre and the WT mice expressed the intact AR form whereas the ARKO mice showed AR deletion form, smaller than the intact AR (Fig. 1A). Male reproductive organs showed phenotypes consistent with our previous publication (Yeh et al., 2002). The external genitalia showed feminized appearance, microphallus, and the urethra showed hypospadia in male ARKO mice. The scrotum of the ARKO mice was poorly developed and showed female phenotype. ARKO mice also showed agenesis of vas deferens, epididymis, seminal vesicle, testis, and prostate organs (Fig. 1B). ARKO mice also had smaller hearts than WT mice and this phenotype was determined by heart weight/body weight (Fig. 1C). Consistent with previous publications (Kang et al., 2008), ARKO mice show osteoporosis, less trabecular bone formation than WT (Fig. 1D) and obesity, larger white and brown adipocytes than WT mice (Fig. 1E). ARKO mice also exhibit more fatty marrow than WT mice (Fig. 1E). Infertility and dramatic decreases in DHT levels were shown in ARKO mice (Figs. 1F and G). Similar phenotypes were also observed from ARKO mice that were generated by crossing floxed AR/AR female mice with male mice expressing cre recombinase driven by β-actin promoter (data not shown).

Bone developmental genes are down-regulated in ARKO BMSCs

BMSCs contain a subset of stem cells that are able to form osteoblasts and marrow adipocytes, and are able to self-renew. To dissect the mechanism by which AR affects stimulation of osteoblasts differentiation, a whole genome microarray analysis was performed. The results revealed that the ARKO BMSCs showed several down-regulated genes in categories of skeletal system development, ossification, bone development, and osteoblast differentiation (Figs. 2A, B, and Supplemental Table 1), whereas no significantly changed up-regulated genes were found in the category of adipose development (Fig. 2A and Supplemental Table 1). To confirm whether the down-regulated genes associated with bone development are correlated with osteogenesis of BMSCs, a mineralization assay testing osteoblast lineage differentiation of BMSCs was performed. Indeed, using alizarin red staining to quantify mineralization, ARKO BMSCs displayed less mineralization than WT BMSCs (Fig. 2C). A similar phenotype was also observed in siRNA-AR-treated human BMSCs with less mineralization than control human BMSCs (Fig. 2G). The ARKO effects in osteogenesis were further confirmed via examining osteogenesis markers expression and the results showed that alkaline phosphatase 2 (Akp2), bone sialoprotein (IBSP), and dentin matrix protein 1 (Dmp1) were expressed at lower level in ARKO BMSCs than WT BMSCs (Figs. 2D–F).

Knockout of AR increases progenitor numbers of BMSCs and their adipogenesis capacity

It has been shown that either increased adipocyte progenitor numbers or enhanced adipogenesis ability of BMSCs can increase the final differentiated adipocyte numbers (Bonyadi et al., 2003; Shin et al., 2009). To clarify how the knockout of AR increases adipogenesis of BMSCs, colony forming efficiency, a rough estimate of the number of skeletal stem/progenitor cells, was performed. ARKO BMSCs exhibited significantly higher numbers of colonies than WT BMSCs as the quantification shows (Fig. 3A). Consistent results were obtained using the adipocyte-derived stromal cells (ADSCs) (Fig. 3B). To determine whether knockout of AR also enhances the adipogenesis potential of BMSCs, an adipogenesis induction experiment was performed. The results revealed that the ARKO BMSCs have more adipocyte formation than the WT BMSCs (Fig. 3C). Expression profiles of adipogenesis markers exhibited that fatty acid binding protein 4 (aP2), lipoprotein lipase (LPL), and PPARγ, were shown to be significantly up-regulated in ARKO BMSCs (Fig. 3D). We also observed a similar phenotype when we knocked down AR in human BMSCs. Knockdown of AR in human BMSCs promoted adipogenesis and adipogenic markers (Figs. 3E and F).

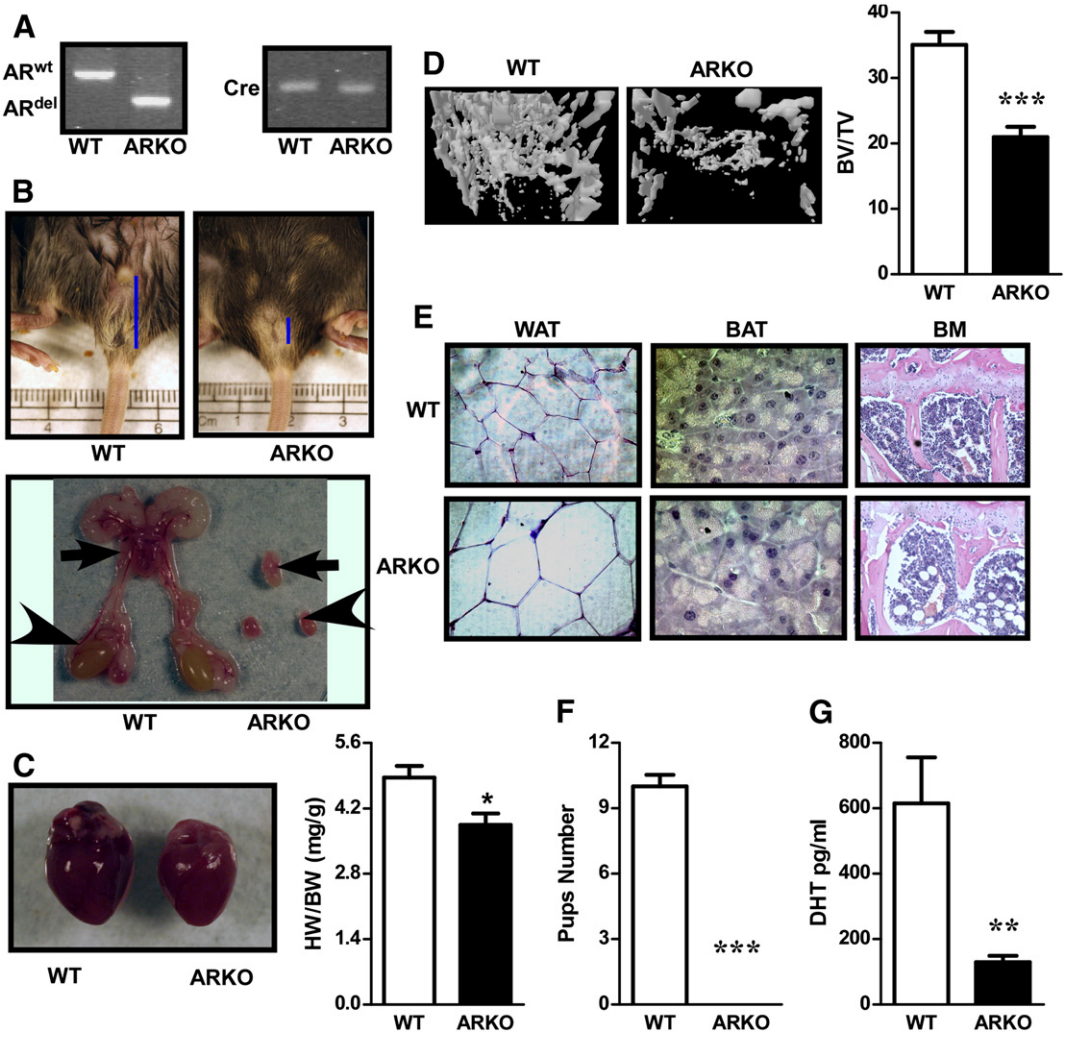

Figure 1 ARKO mice exhibit osteoporosis and enlarged adiocytes. (A) Genotyping of WT and ARKO mice. AR^{wt} indicates intact AR and AR^{del} is mutant AR. Cre bands are cre recombinase positive. (B) Upper panel: The external genitalia of male WT and ARKO mice. Lower panel: The internal genitalia of WT and ARKO mice. Arrowheads and arrows indicate testis and bladder, respectively. (C) Representative heart images of WT and ARKO mice. Graph is the quantification of heart weight over body weight (HW/BW). (D) Representative images of trabecular bone from WT and ARKO mice. Graph is bone volume over tissue volume (BV/TV). (E) Representative images of white adipose tissues and brown adipose tissues of WT and ARKO mice. (F) Fertility test in WT and ARKO mice by measuring numbers of pups/litter number. (G) DHT concentrations in WT and ARKO mice. For all studies, n = 6 from either WT or ARKO mice. *, p value < 0.05. **, p value < 0.001. ***, p value < 0.0001. p values were generated with the Student's t test.

Together, we can conclude that AR deficiency in BMSCs could promote their ability to increase progenitor cell numbers and adipogenesis, and thereby increase the number of differentiated adipocytes.

Knockout of AR inhibits IGFBP3 activation of pAkt

Although we clearly documented that the knockout of AR can stimulate BMSC adipogenesis potential, the mechanism

Figure 2 Identifying key regulators involved in AR-mediated osteogenesis and adipogenesis in BMSCs. (A) Classifications of top 10 Categories of signature genes that are positively correlated or regulated by AR. Highlighted are genes previously reported to promote osteogenesis (blue color) and inhibit adipogenesis (*). (B) AR-mediated key factors in bone development. Black letters within red objects are major categories of key factors. Green letters beside the red objects are full gene names. (C) Osteogenesis determination by using alizarin red staining in WT and ARKO BMSCs. (D) Akp2, (E) IBSP, and (F) Dmp1 expression were measured in WT and ARKO BMSCs after 30 days of osteogenesis induction. (G) Alizarin red staining was performed in human bone marrow stromal cells (hBMSCs), which were manipulated with siRNA scramble control (sc) or siRNA-AR (siAR). Quantitation is shown in the graph. *, p value < 0.05, ***, p value < 0.0001. p values were generated with the Student's t test.

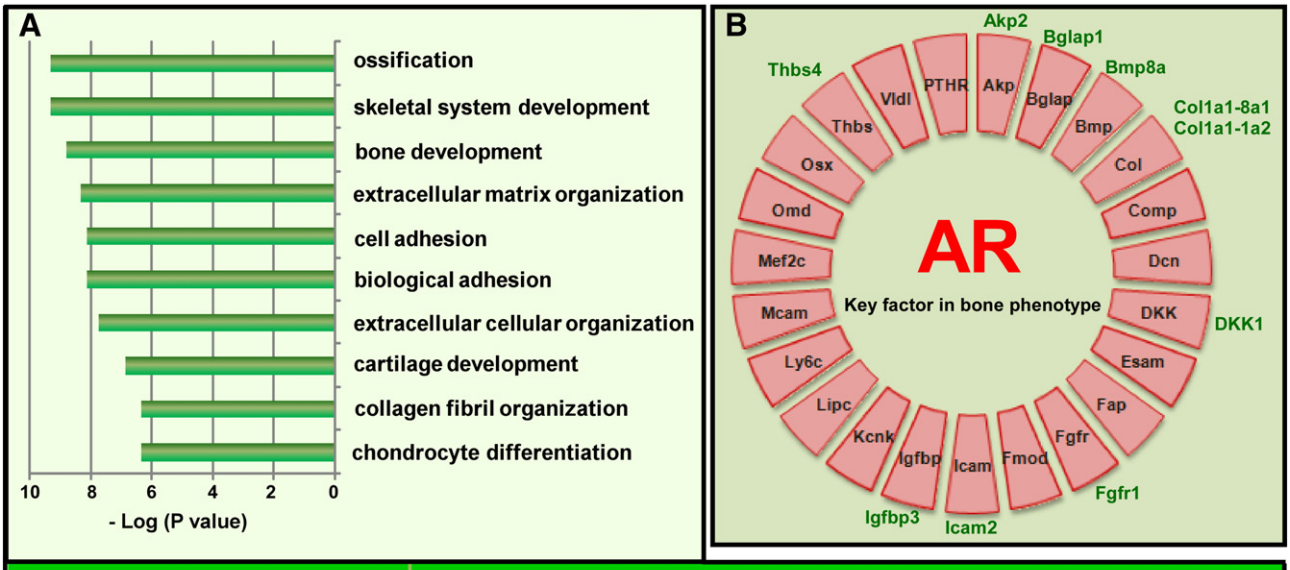

Category	Gene Symbol
ossification	*Sp7; Bmp8a; Col1a1; Col2a1; Col8a1; Dmp1; Igfbp3*; PTH1R*
skeletal system development	*Sp7; Bmp8a; Col1a1; Col2a1; Col5a1; Col6a1; Col6a2; Col8a1; Dmp1; Fgfr1; Igfbp3*; MEF2C; PTH1R*
bone development	*Sp7; Bmp8a; Col1a1; Col2a1; Col8a1; Dmp1; Igfbp3*; PTH1R*
extracellular matrix organization	*Ace; Col2a1; Col5a1; Col5a2; Col6a1; Col6a2; Col8a1; Dmp1; Olfml2b; SERPINH1; IBSP*
cell adhesion	*WISP1; adam12; agt; cdh5; comP; cgref1; Col2a1; Col5a1; Col6a2; Col11a1; Col11a2; Col13a1; Col18a1; Esam; Icam2; MCAM; NRP2; omd; IBSP; TNC; thbs4*
biological adhesion	*WISP1; adam12; agt; cdh5; comP; cgref1; Col2a1; Col5a1; Col6a2; Col11a1; Col11a2; Col13a1; Col18a1; Esam; Icam2; MCAM; NRP2; omd; IBSP; TNC; thbs4*
extracellular cellular organization	*agt; Col2a1; Col5a1; Col5a2; Col11a1; Col11a2; Col18a1; Dmp1; Olfml2b; SERPINH1; IBSP; TNC*
cartilage development	*Bmp8a; Col1a1; Col2a1; Col11a1; Col11a2; Fgfr1; MEF2C; PTH1R; SATB2*
collagen fibril organization	*Col2a1; Col11a1; Col11a2; Fgfr1; MEF2C; PTH1R*
chondrocyte differentiation	*Col2a1; Col5a1; Col5a2; Col11a1; Col11a2; SERPINH1*

Genes highlighted in blue are reported to be functional positively correlated to bone development & * reported to negatively regulate adipocyte differentiation.

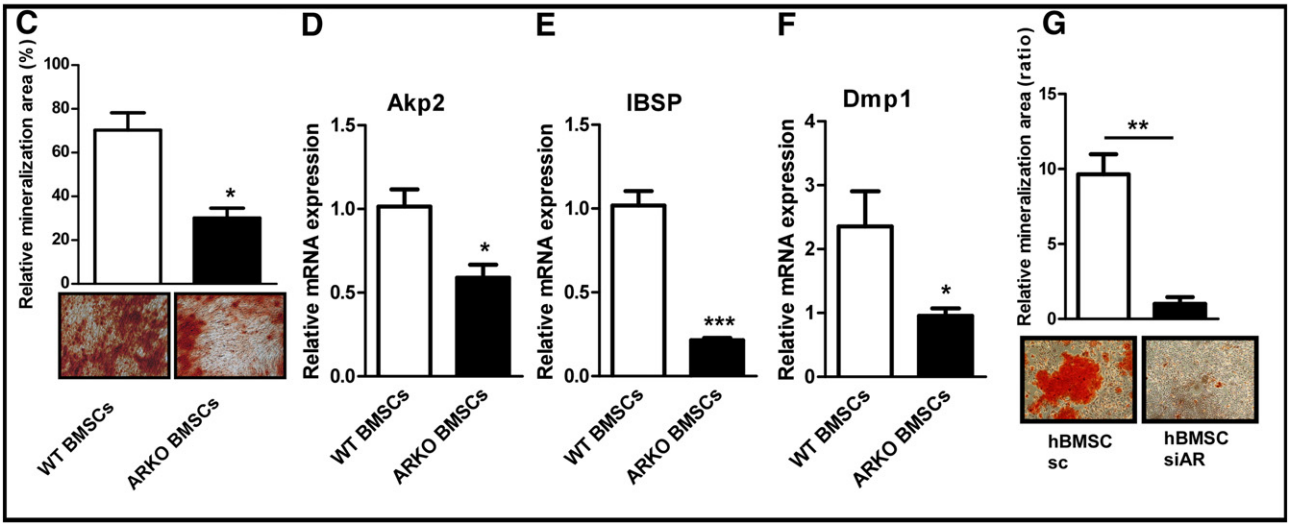

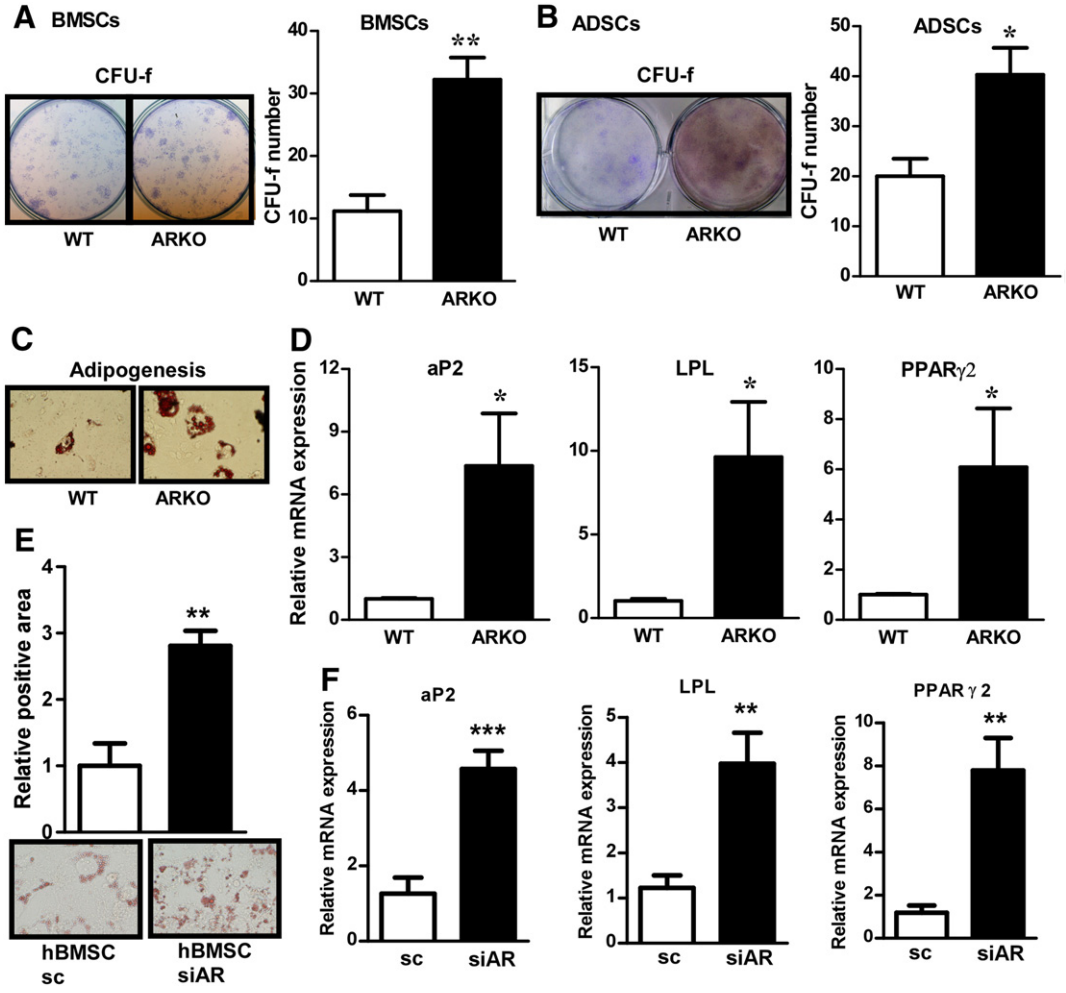

Figure 3 AR deficiency increases progenitors and adipogenic potentials of stromal cells. (A) Representative images of colonies in WT and ARKO mice. Graph on the right is quantification of colony numbers. (B) Colony forming efficiency analysis was performed in WT and ARKO ADSCs. Graph on the right is the quantification of colony numbers. (C) Adipogenesis analysis of WT and ARKO BMSCs using Oil Red O staining. (D) aP2, LPL, and PPARγ2 mRNA levels were determined to quantify the extents of adipogenesis in WT and ARKO BMSCs. (E) Oil Red O staining was performed in hBMSCs, which were manipulated with scramble control (sc) or siRNA-AR (siAR). Quantitation result is shown in the graph. (F) aP2, LPL, and PPARγ2 were determined in hBMSCs, which were manipulated with either sc or siAR. *, p value < 0.05. **, p value < 0.001. p values were generated with the Student's t test.

is not clear. It has been shown that insulin-like growth factors (IGFs) can promote adipogenesis (Jia and Heersche, 2000; Oka et al., 1984). IGFBPs have been shown to suppress adipogenesis (Baxter and Twigg, 2009; Chan et al., 2009; Rajkumar et al., 1999) through either sequestering IGFs to prevent its binding to IGF receptors (IGFRs) or interacting with PPARγ to disrupt its adipogenic function (Chan et al., 2009). Elevated IGFBP3 all leads to insulin resistance in adipocytes via suppressing IGF1 induced pAkt (Chan et al., 2005). In our microarray analysis, we found that knockout of AR in BMSCs suppressed IGFBP3 expression, suggesting that AR might inhibit IGF1-induced adipogenesis through promoting IGFBP3. We therefore decided to further explore IGFBP3 related genes in WT and ARKO BMSCs. The q-RTPCR results exhibited that the knockout of AR suppressed IGFBP3, but increased IGF2 (Fig. 4A). There was no significant difference in expressions of IGF1, IGF1R, and IGF2R in ARKO and WT BMSCs (Fig. 4A). The IGFBP3 protein expression was decreased in ARKO BMSCs (Fig. 4D). Similarly, knockdown of AR in human BMSCs also resulted in suppression of IGFBP3 at the mRNA level (Fig. 4B) and at the protein level (Fig. 4C). To further dissect the potential down-stream gene cascade modulated by the AR mediated IGFBP3 signaling to influence adipogenesis process, we investigated Akt, Erk1/2, and JNK pathways in BMSCs, since it has been shown that Akt, Erk1/2, and JNK are involved in adipogeneis (Bluher et al., 2009; Bost et al., 2005; Prusty et al., 2002; Xu and Liao, 2004; Zhang et al., 2009). Interestingly, the results showed that IGFBP3 negatively correlated with activation of Akt, but not Erk1/2 and JNK (Figs. 4D–F). The quantification results further validated this conclusion by showing the significant difference in ratio of pAkt over Akt, but not the ratios of pErk1/2 over Erk1/2 and pJNK over JNK (Figs. 4D–F). The consistent down-regulation of pAkt by AR was also observed in ADSCs (Fig. 4G). In order to determine whether the pAkt is regulated by AR mediated IGFBP3 signaling, the IGF2 inhibitor (Chromeceptin) was used to

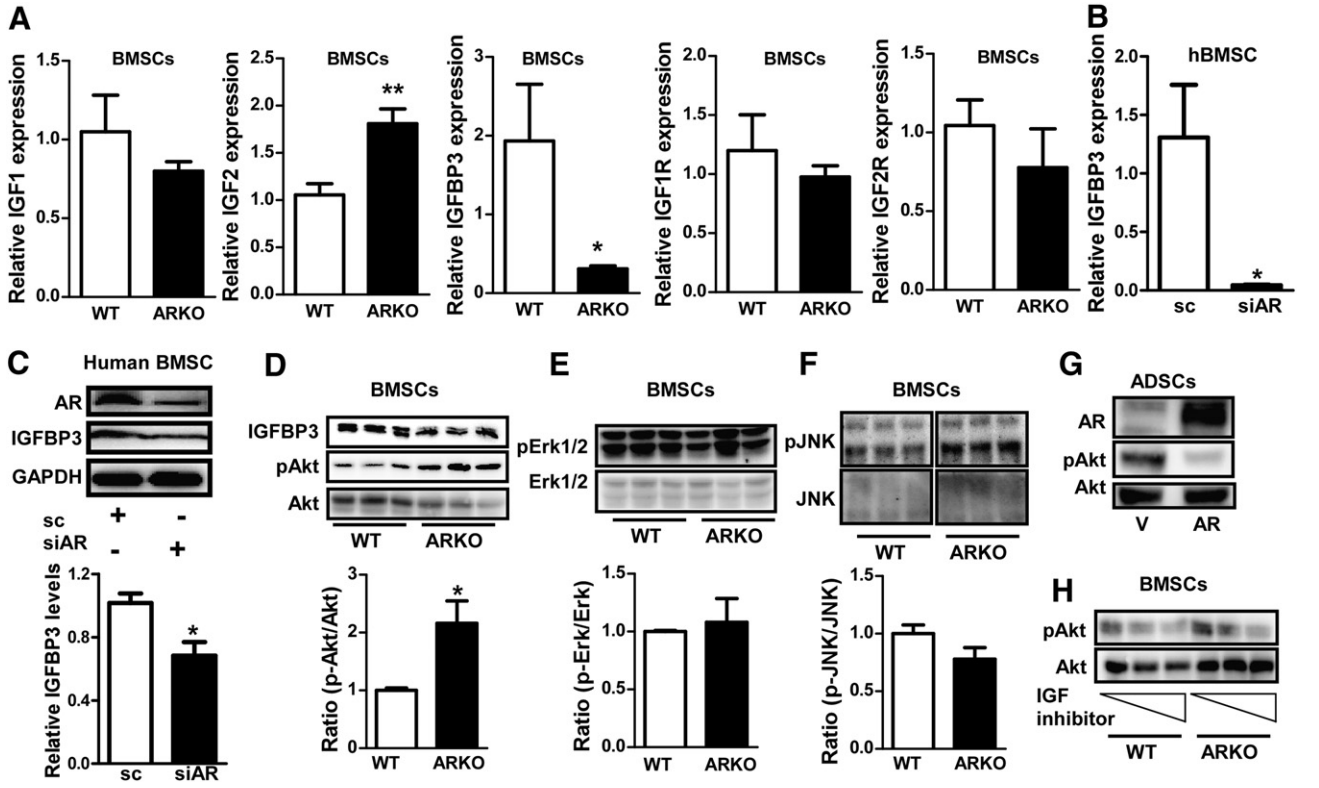

Figure 4 AR deficiency suppresses activation of Akt by IGFBP3 in BMSCs. (A) IGF1, IGF2, IGFBP3, IGF1R, and IGF2R were measured using qRT-PCR in WT and ARKO BMSCs. n = 8 from either WT or ARKO mice. (B) IGFBP3 mRNA and (C) protein expression were examined in hBMSC-sc and hBMSC-siAR. (D–F) IGFBP3, Akt, pAkt, Erk1/2, pErk1/2, JNK, and pJNK, were determined in BMSCs from 3 WT and ARKO mice. Quantification ratios of pAkt over Akt (pAkt/Akt), pErk1/2 over Erk1/2 (pErk/Erk), and pJNK over JNK (pJNK/JNK) were determined and shown in graphs below gel images. (G) AR, pAkt, and Akt were measured in ARKO ADSCs transfected with vector (V) and AR plasmids. (H) IGF inhibitor effects on Akt activation were tested in WT and ARKO BMSCs. pAkt expression is dose dependently inhibited by IGF inhibitor in WT and ARKO BMSCs. *, p value < 0.05. p values were generated with the Student's t test.

mask AR effects (Ma et al., 2011), since it has been shown that IGF2 is regulated by IGFBP3. We found pAkt was increased in ARKO BMSCs and the IGF inhibitors successfully masked AR mediated IGFBP3 signaling effects on pAkt expression in WT and ARKO BMSCs (Hashimoto et al., 1997; Oesterreicher et al., 2005; Wang et al., 2006; Xu et al., 1996) (Fig. 4H). Taken together, the results in Fig. 4 clearly showed that knockout of AR suppressed IGFBP3 activation of Akt signaling and influenced the adipogenesis process.

AR enhances IGFBP3 transcription through direct promoter binding

Although the IGFBP3-mediated activation of Akt signaling is clear, the mechanism of AR regulation of IGFBP3 remains in question. Therefore, we performed a promoter search to identify putative AR binding elements (AREs) located on the promoter region of IGFBP3. We found two potential AREs, AGAAAAnnnnTGTCCT and ACTAAAnnnTGTTCT, which are located at −794 to −819 and −1802 to −1816, respectively (Fig. 5A). We constructed a pGL3-luciferase reporter containing the IGFBP3 promoter region to directly test the transcriptional regulation of IGFBP3 by AR (Fig. 5B). Using the MMTV-luciferase construct which contains a strong ARE as a positive control, we found AR enhanced IGFBP3 promote transactivation with 2 fold induction in the presence of androgen (Fig. 5C), suggesting that AR might directly bind to the IGFBP3 promoter to modulate IGFBP3 transcription. To further clarify whether AR directly binds to the IGFBP3 promoter, we used a ChIP assay to validate the potential ARE sites. The input positive controls of WT and ARKO BMSCs showed clear bands when using specific primers to amplify ARE 2 located in the IGFBP3 promoter region. We found that AR in WT BMSCs can bind to the ARE 2 of IGFBP3 promoter region, but such binding was barely detected when the ARKO BMSCs were used in the assay (Fig. 5D), suggesting that AR in WT BMSCs was functional and able to regulate IGFBP3 transcriptionally through direct binding to the IGFBP3 promoter region.

Blocking of pAkt and IGF signaling reverses ARKO effects on adipogenesis

We have identified that AR might stimulate IGFBP3 to affect pAkt and IGF signaling. However, it was not clear whether AR modulated adipogenesis through these pathways. To further validate whether the AR mediated adipogenesis is pAkt and IGF dependent, we used a pAkt inhibitor (LY294002), an IGF1 inhibitor (Picropodophyllin, PPP), and an IGF2 inhibitor (Chromeceptin, Chrome) to block

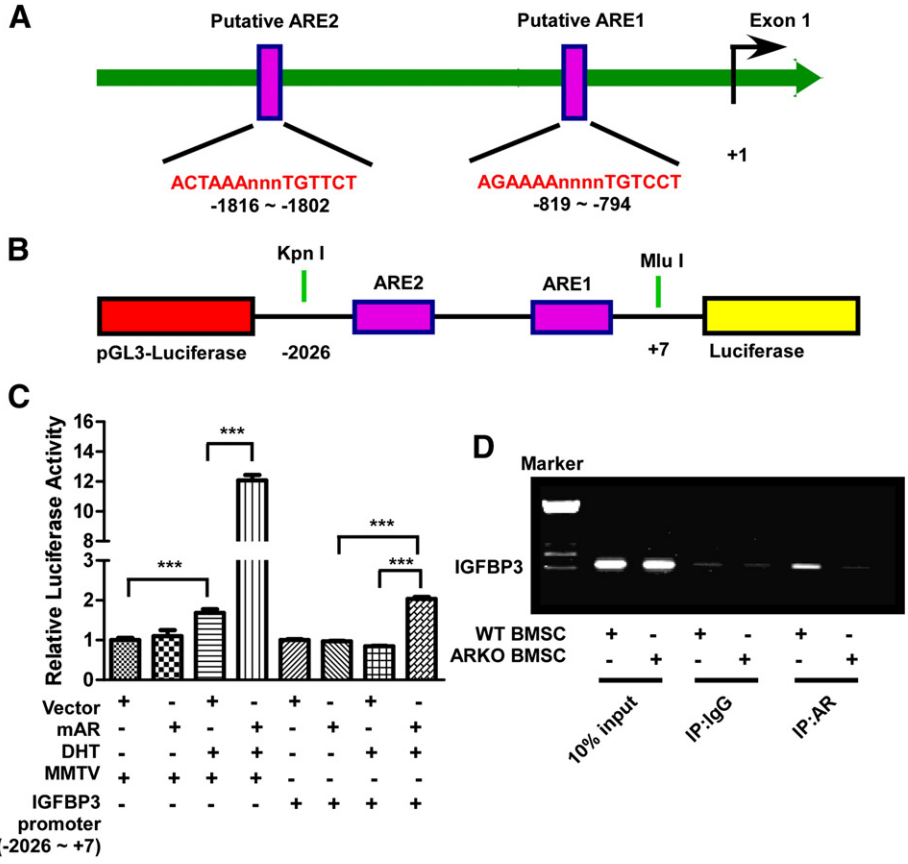

Figure 5 AR modulates IGFBP3 through promoter regulation. (A) Illustration of the IGFBP3 promoter region and 2 putative AREs, ARE1 located from −819–794 and ARE2 located from −1816–1802. (B) Map of the constructed pGL3-IGFBP3 luciferase. A segment of IGFBP3 promoter is from the location −2026 to +7. The two insertion sites are Kpn I and Mlu I. (C) Luciferase assays of MMTV-luciferase (MMTV) and pGL3-IGFBP3-luciferase (IGFBP3 promoter) were performed in HEK-293T cells. 1 ng pRL-Tk was used as control for luciferase. 0.5 μg vector, mAR, MMTV, and IGFBP3 promoter were transfected into HEK-293T cells either in the presence or absence of 10 nM DHT. (D) Chromatin immunoprecipitation assay was performed in WT and ARKO BMSCs. Non-immune 10% input served as positive control for IGFBP3 primers specific for ARE2. IgG was used to pull down chromatin complex as a negative control. AR antibody was used to pull down chromatin complex as experimental targets. ***, p value < 0.0001. p values were generated with the Student's t test.

ARKO-mediated adipogenesis (Choi et al., 2006; Girnita et al., 2008; Menu et al., 2007). We found that ARKO BMSCs consistently had higher numbers of Oil Red O positively stained adipocytes than WT BMSCs in the presence of vehicle in three different experimental settings (Figs. 6A–C). The adipogenesis markers, LPL, aP2, and PPARγ2 were significantly increased in ARKO BMSCs compared to WT BMSCs (Figs. 6A–C). However, treatment with the pAkt inhibitor masked the difference in Oil Red O positively stained adipocytes numbers between WT and ARKO BMSCs, and significantly suppressed expression of LPL, aP2, and PPARγ2 compared to vehicle-treated ARKO BMSCs (Fig. 6A). Treatment with the two IGF inhibitors also significantly abolished the ARKO effect and we no longer observed differences in Oil Red O positively stained adipocytes numbers (Figs. 6B, C). The LPL, aP2, and PPARγ2 expression results confirmed the staining results. The observed difference in adipogenesis markers between WT and ARKO BMSCs (Fig. 6) disappeared after treatment with these inhibitors, suggesting that the AR mediated suppression of adipogenesis is partially mediated by IGF pathways.

Discussion

Gender differences have been suggested in osteoporosis and obesity for several decades. Although the effects of estrogen and estrogen receptor signaling on osteoporosis and obesity have been extensively investigated (Becker, 2010; Gennari et al., 2007; Mauvais-Jarvis, 2011; Moverare et al., 2003; Smith, 2005; Yi et al., 2008), the effects of androgen and AR signaling on obesity and osteoporosis remain elusive. Previous studies mainly focused on androgen and AR signaling in studies relevant to osteoporosis, such as osteoblast differentiation, mineralization, and osteoclast activity. It has been shown that androgen induces osteoblast differentiation and mineralization (Balkan et al., 2005) and AR expression is gradually increased in differentiated osteoblast (Wiren et al., 2002). In orchidectomized mice, DHT treatment could reverse the orchidectomy-induced trabecular bone loss phenotype (Moverare et al., 2003). AR has suppressive functions in osteoclast activity to inhibit the bone resorption (Kawano et al., 2003) and AR deficient mice exhibit a bone loss phenotype in calvarial and femoral bones

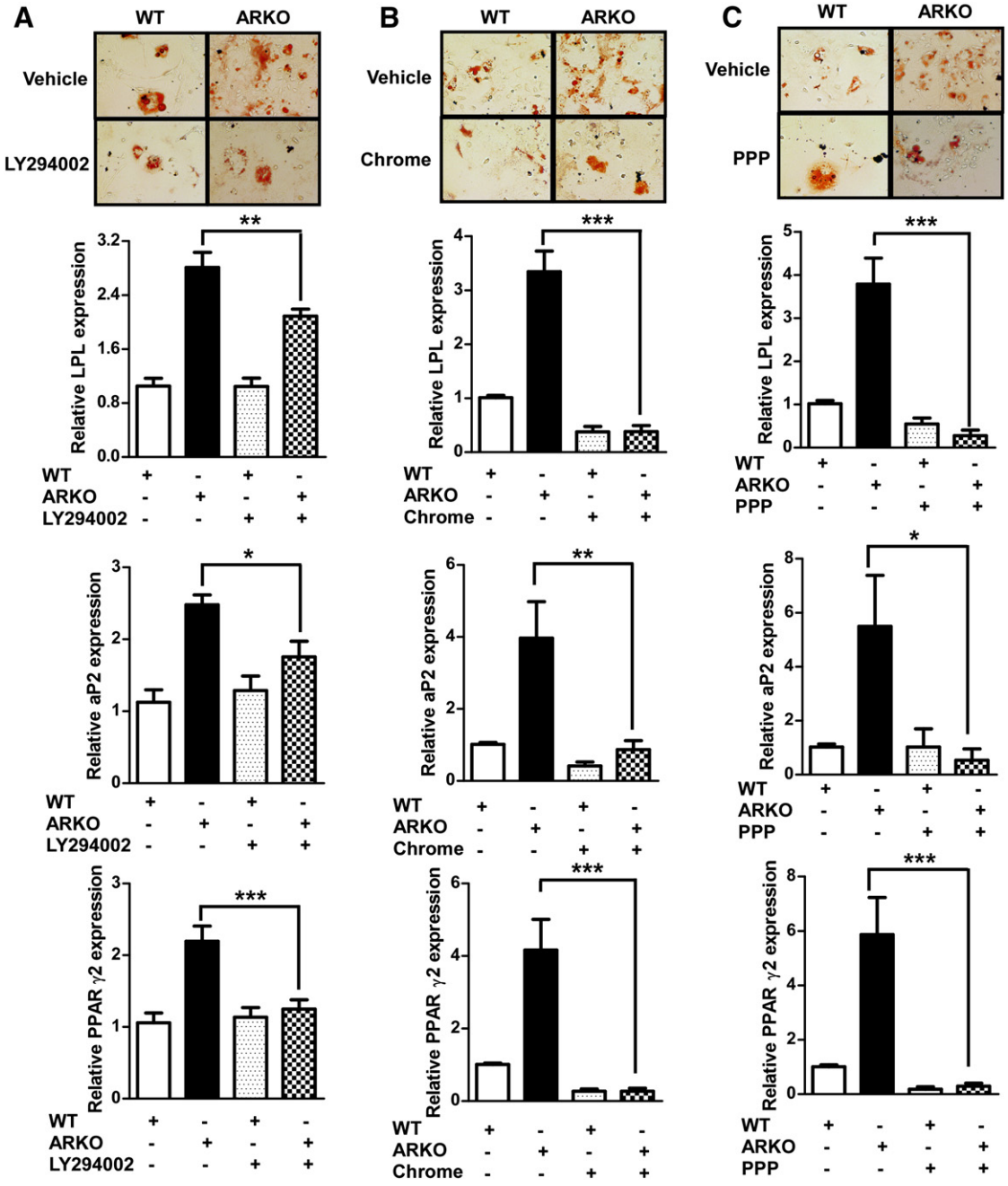

Figure 6 Inhibition of IGFs and Akt signaling pathways reverse the AR deficiency effects on BMSC adipogenesis. (A) Oil Red O staining was used to visualize oil droplets, and qRT-PCR was used to determine adipogenisis markers including LPL, aP2, and PPARγ2 in the differentiated adipocytes from WT and ARKO BMSCs in the presence of 10 μM LY294002 (Akt inhibitor). (B) 1 μM Chromeceptin (Chrome), the IGF inhibitor and (C) 2 μM PPP (IGF I inhibitor) were used to treat WT and ARKO BMSCs, which were under adipogenic induction and the adipogenic differentiation was monitored by Oil Red O staining and qRT-PCR to determine oil droplets and adipogenesis markers. *, p value < 0.05. **, p value < 0.001 ***, p value < 0.0001. p values were generated with the Student's s test.

(Kang et al., 2008; Tsai et al., 2011). Other studies using selective androgen receptor modulators (SARMs) to treat ovariectomized or orchiectomized rats also demonstrated that activation of AR signaling prevents bone loss (Kearbey et al., 2007; Rosen and Negro-Vilar, 2002). In addition, androgenic treatments enhanced apoptosis of osteoblasts resulting in anabolic stimulation of new bone growth both in vitro and in vivo (Wiren et al., 2006). In the present study, we established ARKO mice by breeding EIIa or Actb Cre mice with floxed AR/AR mice and obtained the results that these two kinds of ARKO mice exhibit consistent phenotypes with bone loss. Moreover, our microarray analysis results demonstrated that AR deficiency in BMSCs significantly represses gene categories relevant to bone development and formation including ossification, skeletal system development, and bone development. Our studies on AR signaling in osteogenesis of

BMSCs further support the concept that AR enhances bone growth and inhibits osteoporosis via promoting BMSCs differentiation into bone.

Androgen and AR signaling studies in obesity and adipogenesis have demonstrated that androgen treatments inhibit adipocyte differentiation and body fat formation in both in vitro cell culture and in vivo animal models including rodents and nonhuman primates (Blouin et al., 2008; Singh et al., 2003, 2006; Varlamov et al., 2012; Zhang et al., 2008). Androgen promotes the interactions among β-catenin, AR, and T-cell factor 4 to suppress adipogenic differentiation in 3T3-L1 cells (Singh et al., 2006). Androgen inhibits rosiglitazone-induced adipogenesis in human BMSCs (Benvenuti et al., 2012; Gupta et al., 2008). It is clear that androgen inhibits adipogenesis either in preadipocytes from white fat and BMSCs. However, AR is a transcriptional factor that modulates gene expressions to coordinate body development and function. It is essential to systematically analyze how AR signaling in BMSCs transcriptionally affects gene expressions in order to fully decipher AR function in adipogenesis of BMSCs. Although previous studies have compared gene changes between vehicle and androgen treatments in adipocytes, none of them performed comparison to BMSCs (Nantermet et al., 2008; Zhang et al., 2008). Furthermore, it has been shown that charcoal stripped (CS) fetal bovine serum (FBS) used in androgen treatment studies still has residual testosterone levels (FBS: 2.7 ± 0.13 nM, CS-FBS: 1.1 ± 0.39 nM) (Goldman-Johnson et al., 2008). In this study, Goldman-Johnson et al. also demonstrated that embryonic stem cells can synthesize testosterone at 0.53–1.38 nM per 24 h. It does not seem to be suitable to dissect AR signaling in adipogenesis of BMSCs and white adipocyte derived preadipocytes by comparing vehicle and androgen treatment in these conditions. Therefore, comparing gene changes in BMSCs from WT and ARKO mice would elaborate more accurate detailed molecular mechanism of androgen and AR in the adipogenesis of BMSCs.

In our present study, we used BMSCs from WT and ARKO mice and performed microarray assays to systematically analyze the gene expression changes. We found AR depletion in BMSCs significantly decreased expression of genes associated with bone development. However, the canonical adipogenesis pathway in BMSCs was not directly altered by AR knockout. Interestingly, depletion of AR in BMSCs increased the number of progenitors and their adipogenic potential to enhance adipocyte differentiation. When we analyzed AR down-regulated genes, we hypothesized that IGFBP3 could be a potential candidate modulating the effect, since IGFBP3 might modulate IGF pathways to inhibit adipogenesis. Indeed, we observed that ARKO BMSCs expressed lower levels of IGFBP3, which in turn, activated Akt signaling (induced by IGF pathways) as compared to WT BMSCs. The luciferase and ChIP assays results both demonstrated that AR positively and directly regulated IGFBP3 expression. Using IGF inhibitors to treat WT and ARKO BMSCs, the ARKO effect in enhancing pAkt expression was reversed, suggesting that AR promotes IGFBP3 to repress IGF pathways and then to reduce pAkt activation, resulting in less adipocyte differentiation. This conclusion was further supported by the inhibitor studies using pAkt, IGF1, and IGF2 inhibitors that could block adipogenesis of WT and ARKO BMSCs. The results showed that all three inhibitors successfully reversed the AR knockout effect in adipocyte differentiation through antagonizing Akt activation modulated by AR-IGF–IGFBP3 signaling.

In summary, we demonstrated that AR promoted osteogenesis and inhibited adipogenesis in BMSCs. Using microarray analysis, we found AR positively regulates gene categories relevant to bone development. This observation partially explains the gender difference in osteoporosis, since the female gender has lower androgen and AR signaling. In the molecular mechanism study, we found AR directly modulates IGFBP3 expression via promoter regulation. In AR deficient BMSCs, down-regulated IGFBP3 might result in loss of sequestration of IGFs and allow IGFs to activate pAkt to stimulate adipogenesis. Meanwhile, treatments with pAkt, IGF1 and IGF2 inhibitors successfully reversed the AR depletion effects on adipogenesis, suggesting that the AR mediated adipogenesis is through the Akt and IGF pathways. Although there might be other pathways contributing to the AR-mediated suppression of BMSCs adipogenesis, our conclusions at least partially explain how AR influences BMSCs adipogenesis. The study provides the information related to AR mediated osteogenesis and adipogenesis of BMSCs and this information may be relevant for clinical management of osteoporosis.

Acknowledgments

We thank Karen Wolf for the manuscript editing. We thank Dr. Tzong-Jen Sheu's help for the tissue blocks that involved bone marrow sections. This work was supported by NIH grants (CA122840 and CA156700), and the Taiwan Department of Health Clinical Trial and Research Center of Excellence (DOH99-TD-B-111-004) to China Medical University, Taiwan.

Appendix A. Supplementary data

Supplementary data to this article can be found online at http://dx.doi.org/10.1016/j.scr.2013.06.001.

Reference

Alibhai, S.M., Yun, L., Cheung, A.M., Paszat, L., 2012. Screening for osteoporosis in men receiving androgen deprivation therapy. JAMA 307, 255–256.

Balkan, W., Burnstein, K.L., Schiller, P.C., Perez-Stable, C., D'Ippolito, G., Howard, G.A., Roos, B.A., 2005. Androgen-induced mineralization by MC3T3-E1 osteoblastic cells reveals a critical window of hormone responsiveness. Biochem. Biophys. Res. Commun. 328, 783–789.

Baxter, R.C., Twigg, S.M., 2009. Actions of IGF binding proteins and related proteins in adipose tissue. Trends Endocrinol. Metab. 20, 499–505.

Becker, C., 2010. Another selective estrogen-receptor modulator for osteoporosis. N. Engl. J. Med. 362, 752–754.

Benvenuti, S., Cellai, I., Luciani, P., Deledda, C., Saccardi, R., Mazzanti, B., Dal Pozzo, S., Serio, M., Peri, A., 2012. Androgens and estrogens prevent rosiglitazone-induced adipogenesis in human mesenchymal stem cells. J. Endocrinol. Investig. 35, 365–371.

Bianco, P., Kuznetsov, S.A., Riminucci, M., Gehron Robey, P., 2006. Postnatal skeletal stem cells. Methods Enzymol. 419, 117–148.

Blouin, K., Boivin, A., Tchernof, A., 2008. Androgens and body fat distribution. J. Steroid Biochem. Mol. Biol. 108, 272–280.

Bluher, M., Bashan, N., Shai, I., Harman-Boehm, I., Tarnovscki, T., Avinaoch, E., Stumvoll, M., Dietrich, A., Kloting, N., Rudich, A., 2009. Activated Ask1–MKK4–p38MAPK/JNK stress signaling pathway in human omental fat tissue may link macrophage infiltration to whole-body Insulin sensitivity. J. Clin. Endocrinol. Metab. 94, 2507–2515.

Boling, E.P., 2001. Gender and osteoporosis: similarities and sex-specific differences. J. Gend. Specif. Med. 4, 36–43.

Bonyadi, M., Waldman, S.D., Liu, D., Aubin, J.E., Grynpas, M.D., Stanford, W.L., 2003. Mesenchymal progenitor self-renewal deficiency leads to age-dependent osteoporosis in Sca-1/Ly-6A null mice. Proc. Natl. Acad. Sci. U. S. A. 100, 5840–5845.

Bost, F., Aouadi, M., Caron, L., Binetruy, B., 2005. The role of MAPKs in adipocyte differentiation and obesity. Biochimie 87, 51–56.

Carney, P.I., 2010. Obesity and reproductive hormone levels in the transition to menopause. Menopause 17, 678–679.

Castro-Malaspina, H., Gay, R.E., Resnick, G., Kapoor, N., Meyers, P., Chiarieri, D., McKenzie, S., Broxmeyer, H.E., Moore, M.A., 1980. Characterization of human bone marrow fibroblast colony-forming cells (CFU-F) and their progeny. Blood 56, 289–301.

Chan, S.S., Twigg, S.M., Firth, S.M., Baxter, R.C., 2005. Insulin-like growth factor binding protein-3 leads to insulin resistance in adipocytes. J. Clin. Endocrinol. Metab. 90, 6588–6595.

Chan, S.S., Schedlich, L.J., Twigg, S.M., Baxter, R.C., 2009. Inhibition of adipocyte differentiation by insulin-like growth factor-binding protein-3. Am. J. Physiol. Endocrinol. Metab. 296, E654–E663.

Chiang, C., Chiu, M., Moore, A.J., Anderson, P.H., Ghasem-Zadeh, A., McManus, J.F., Ma, C., Seeman, E., Clemens, T.L., Morris, H.A., et al., 2009. Mineralization and bone resorption are regulated by the androgen receptor in male mice. J. Bone Miner. Res. 24, 621–631.

Choi, Y., Shimogawa, H., Murakami, K., Ramdas, L., Zhang, W., Qin, J., Uesugi, M., 2006. Chemical genetic identification of the IGF-linked pathway that is mediated by STAT6 and MFP2. Chem. Biol. 13, 241–249.

Chuang, K.H., Altuwaijri, S., Li, G., Lai, J.J., Chu, C.Y., Lai, K.P., Lin, H.Y., Hsu, J.W., Keng, P., Wu, M.C., et al., 2009. Neutropenia with impaired host defense against microbial infection in mice lacking androgen receptor. J. Exp. Med. 206, 1181–1199.

Cilotti, A., Falchetti, A., 2009. Male osteoporosis and androgenic therapy: from testosterone to SARMs. Clin. Cases Miner. Bone Metab. 6, 229–233.

Collier, A., Ghosh, S., McGlynn, B., Hollins, G., 2011. Prostate cancer, androgen deprivation therapy, obesity, the metabolic syndrome, type 2 diabetes, and cardiovascular disease: a review. Am. J. Clin. Oncol. 35, 504–509.

Coumoul, X., Shukla, V., Li, C., Wang, R.H., Deng, C.X., 2005. Conditional knockdown of Fgfr2 in mice using Cre-LoxP induced RNA interference. Nucleic Acids Res. 33, e102.

Faith, J.J., Driscoll, M.E., Fusaro, V.A., Cosgrove, E.J., Hayete, B., Juhn, F.S., Schneider, S.J., Gardner, T.S., 2008. Many Microbe Microarrays Database: uniformly normalized Affymetrix compendia with structured experimental metadata. Nucleic Acids Res. 36, D866–D870.

Freeman, E.W., Sammel, M.D., Lin, H., Gracia, C.R., 2010. Obesity and reproductive hormone levels in the transition to menopause. Menopause 17, 718–726.

Galvao, D.A., Spry, N.A., Taaffe, D.R., Newton, R.U., Stanley, J., Shannon, T., Rowling, C., Prince, R., 2008. Changes in muscle, fat and bone mass after 36 weeks of maximal androgen blockade for prostate cancer. BJU Int. 102, 44–47.

Gennari, L., Merlotti, D., Valleggi, F., Martini, G., Nuti, R., 2007. Selective estrogen receptor modulators for postmenopausal osteoporosis: current state of development. Drugs Aging 24, 361–379.

Girnita, A., All-Ericsson, C., Economou, M.A., Astrom, K., Axelson, M., Seregard, S., Larsson, O., Girnita, L., 2008. The insulin-like growth factor-I receptor inhibitor picropodophyllin causes tumor regression and attenuates mechanisms involved in invasion of uveal melanoma cells. Acta Ophthalmol. 86, 26–34 (Thesis 4).

Goldman-Johnson, D.R., de Kretser, D.M., Morrison, J.R., 2008. Evidence that androgens regulate early developmental events, prior to sexual differentiation. Endocrinology 149, 5–14.

Gupta, V., Bhasin, S., Guo, W., Singh, R., Miki, R., Chauhan, P., Choong, K., Tchkonia, T., Lebrasseur, N.K., Flanagan, J.N., et al., 2008. Effects of dihydrotestosterone on differentiation and proliferation of human mesenchymal stem cells and preadipocytes. Mol. Cell. Endocrinol. 296, 32–40.

Hashimoto, R., Ono, M., Fujiwara, H., Higashihashi, N., Yoshida, M., Enjoh-Kimura, T., Sakano, K., 1997. Binding sites and binding properties of binary and ternary complexes of insulin-like growth factor-II (IGF-II), IGF-binding protein-3, and acid-labile subunit. J. Biol. Chem. 272, 27936–27942.

Huang da, W., Sherman, B.T., Lempicki, R.A., 2009. Systematic and integrative analysis of large gene lists using DAVID bioinformatics resources. Nat. Protoc. 4, 44–57.

Huang, C.K., Lee, S.O., Lai, K.P., Ma, W.L., Lin, T.H., Tsai, M.Y., Luo, J., Chang, C., 2012. Targeting androgen receptor in bone marrow mesenchymal stem cells leads to better transplantation therapy efficacy in liver cirrhosis. Hepatology 57, 1550–1563.

Jia, D., Heersche, J.N., 2000. Insulin-like growth factor-1 and -2 stimulate osteoprogenitor proliferation and differentiation and adipocyte formation in cell populations derived from adult rat bone. Bone 27, 785–794.

Kang, H.Y., Shyr, C.R., Huang, C.K., Tsai, M.Y., Orimo, H., Lin, P.C., Chang, C., Huang, K.E., 2008. Altered TNSALP expression and phosphate regulation contribute to reduced mineralization in mice lacking androgen receptor. Mol. Cell. Biol. 28, 7354–7367.

Kawano, H., Sato, T., Yamada, T., Matsumoto, T., Sekine, K., Watanabe, T., Nakamura, T., Fukuda, T., Yoshimura, K., Yoshizawa, T., et al., 2003. Suppressive function of androgen receptor in bone resorption. Proc. Natl. Acad. Sci. U. S. A. 100, 9416–9421.

Kearbey, J.D., Gao, W., Narayanan, R., Fisher, S.J., Wu, D., Miller, D.D., Dalton, J.T., 2007. Selective Androgen Receptor Modulator (SARM) treatment prevents bone loss and reduces body fat in ovariectomized rats. Pharm. Res. 24, 328–335.

Keto, C.J., Aronson, W.J., Terris, M.K., Presti, J.C., Kane, C.J., Amling, C.L., Freedland, S.J., 2012. Obesity is associated with castration-resistant disease and metastasis in men treated with androgen deprivation therapy after radical prostatectomy: results from the SEARCH database. BJU Int. 110, 492–498.

Khosla, S., Melton III, L.J., Riggs, B.L., 1999. Osteoporosis: gender differences and similarities. Lupus 8, 393–396.

Lai, J.J., Lai, K.P., Chuang, K.H., Chang, P., Yu, I.C., Lin, W.J., Chang, C., 2009. Monocyte/macrophage androgen receptor suppresses cutaneous wound healing in mice by enhancing local TNF-alpha expression. J. Clin. Invest. 119, 3739–3751.

Lai, K.P., Yamashita, S., Huang, C.K., Yeh, S., Chang, C., 2012. Loss of stromal androgen receptor leads to suppressed prostate tumourigenesis via modulation of pro-inflammatory cytokines/chemokines. EMBO Mol. Med. 4, 791–807.

Lee, S.O., Ma, Z., Yeh, C.R., Luo, J., Lin, T.H., Lai, K.P., Yamashita, S., Liang, L., Tian, J., Li, L., et al., 2012. New therapy targeting differential androgen receptor signaling in prostate cancer stem/progenitor vs. non-stem/progenitor cells. J. Cell Biol. 5, 14–26.

Lufkin, E.G., Wahner, H.W., O'Fallon, W.M., Hodgson, S.F., Kotowicz, M.A., Lane, A.W., Judd, H.L., Caplan, R.H., Riggs, B.L., 1992. Treatment of postmenopausal osteoporosis with transdermal estrogen. Ann. Intern. Med. 117, 1–9.

Ma, N., Wang, X., Qiao, Y., Li, F., Hui, Y., Zou, C., Jin, J., Lv, G., Peng, Y., Wang, L., et al., 2011. Coexpression of an intronic microRNA and its host gene reveals a potential role for miR-483-5p as an IGF2 partner. Mol. Cell. Endocrinol. 333, 96–101.

Mauvais-Jarvis, F., 2011. Estrogen and androgen receptors: regulators of fuel homeostasis and emerging targets for diabetes and obesity. Trends Endocrinol. Metab. 22, 24–33.

Menu, E., Jernberg-Wiklund, H., De Raeve, H., De Leenheer, E., Coulton, L., Gallagher, O., Van Valckenborgh, E., Larsson, O., Axelson, M., Nilsson, K., et al., 2007. Targeting the IGF-1R using picropodophyllin in the therapeutical 5T2MM mouse model of multiple myeloma: beneficial effects on tumor growth, angiogenesis, bone disease and survival. Int. J. Cancer 121, 1857–1861.

Moverare, S., Venken, K., Eriksson, A.L., Andersson, N., Skrtic, S., Wergedal, J., Mohan, S., Salmon, P., Bouillon, R., Gustafsson, J.A., et al., 2003. Differential effects on bone of estrogen receptor alpha and androgen receptor activation in orchidectomized adult male mice. Proc. Natl. Acad. Sci. U. S. A. 100, 13573–13578.

Nantermet, P., Harada, S., Liu, Y., Cheng, S., Johnson, C., Yu, Y., Kimme, D., Holder, D., Hodor, P., Phillips, R., et al., 2008. Gene expression analyses in cynomolgus monkeys provides mechanistic insight into high-density lipoprotein-cholesterol reduction by androgens in primates. Endocrinology 149, 1551–1561.

Notini, A.J., McManus, J.F., Moore, A., Bouxsein, M., Jimenez, M., Chiu, W.S., Glatt, V., Kream, B.E., Handelsman, D.J., Morris, H.A., et al., 2007. Osteoblast deletion of exon 3 of the androgen receptor gene results in trabecular bone loss in adult male mice. J. Bone Miner. Res. 22, 347–356.

Oesterreicher, S., Blum, W.F., Schmidt, B., Braulke, T., Kubler, B., 2005. Interaction of insulin-like growth factor II (IGF-II) with multiple plasma proteins: high affinity binding of plasminogen to IGF-II and IGF-binding protein-3. J. Biol. Chem. 280, 9994–10000.

Oka, Y., Mottola, C., Oppenheimer, C.L., Czech, M.P., 1984. Insulin activates the appearance of insulin-like growth factor II receptors on the adipocyte cell surface. Proc. Natl. Acad. Sci. U. S. A. 81, 4028–4032.

Prusty, D., Park, B.H., Davis, K.E., Farmer, S.R., 2002. Activation of MEK/ERK signaling promotes adipogenesis by enhancing peroxisome proliferator-activated receptor gamma (PPARgamma) and C/EBPalpha gene expression during the differentiation of 3T3-L1 preadipocytes. J. Biol. Chem. 277, 46226–46232.

Rajkumar, K., Modric, T., Murphy, L.J., 1999. Impaired adipogenesis in insulin-like growth factor binding protein-1 transgenic mice. J. Endocrinol. 162, 457–465.

Rosen, C.J., Bouxsein, M.L., 2006. Mechanisms of disease: is osteoporosis the obesity of bone? Nat. Clin. Pract. Rheumatol. 2, 35–43.

Rosen, J., Negro-Vilar, A., 2002. Novel, non-steroidal, selective androgen receptor modulators (SARMs) with anabolic activity in bone and muscle and improved safety profile. J. Musculoskelet. Neuronal. Interact. 2, 222–224.

Ryan, A.S., Nicklas, B.J., Berman, D.M., 2002. Hormone replacement therapy, insulin sensitivity, and abdominal obesity in postmenopausal women. Diabetes Care 25, 127–133.

Sacchetti, B., Funari, A., Michienzi, S., Di Cesare, S., Piersanti, S., Saggio, I., Tagliafico, E., Ferrari, S., Robey, P.G., Riminucci, M., et al., 2007. Self-renewing osteoprogenitors in bone marrow sinusoids can organize a hematopoietic microenvironment. Cell 131, 324–336.

Shin, D.W., Kim, S.N., Lee, S.M., Lee, W., Song, M.J., Park, S.M., Lee, T.R., Baik, J.H., Kim, H.K., Hong, J.H., et al., 2009. (−)-Catechin promotes adipocyte differentiation in human bone marrow mesenchymal stem cells through PPAR gamma transactivation. Biochem. Pharmacol. 77, 125–133.

Singh, R., Artaza, J.N., Taylor, W.E., Gonzalez-Cadavid, N.F., Bhasin, S., 2003. Androgens stimulate myogenic differentiation and inhibit adipogenesis in C3H 10T1/2 pluripotent cells through an androgen receptor-mediated pathway. Endocrinology 144, 5081–5088.

Singh, R., Artaza, J.N., Taylor, W.E., Braga, M., Yuan, X., Gonzalez-Cadavid, N.F., Bhasin, S., 2006. Testosterone inhibits adipogenic differentiation in 3T3-L1 cells: nuclear translocation of androgen receptor complex with beta-catenin and T-cell factor 4 may bypass canonical Wnt signaling to down-regulate adipogenic transcription factors. Endocrinology 147, 141–154.

Smith, M.R., 2005. Selective estrogen receptor modulators to prevent treatment-related osteoporosis. Rev. Urol. 7 (Suppl. 3), S30–S35.

Tsai, M.Y., Shyr, C.R., Kang, H.Y., Chang, Y.C., Weng, P.L., Wang, S.Y., Huang, K.E., Chang, C., 2011. The reduced trabecular bone mass of adult ARKO male mice results from the decreased osteogenic differentiation of bone marrow stroma cells. Biochem. Biophys. Res. Commun. 411, 477–482.

Varlamov, O., White, A.E., Carroll, J.M., Bethea, C.L., Reddy, A., Slayden, O., O'Rourke, R.W., Roberts Jr., C.T., 2012. Androgen effects on adipose tissue architecture and function in nonhuman primates. Endocrinology 153, 3100–3110.

Wang, T.H., Chang, C.L., Wu, H.M., Chiu, Y.M., Chen, C.K., Wang, H.S., 2006. Insulin-like growth factor-II (IGF-II), IGF-binding protein-3 (IGFBP-3), and IGFBP-4 in follicular fluid are associated with oocyte maturation and embryo development. Fertil. Steril. 86, 1392–1401.

Wiren, K.M., Chapman Evans, A., Zhang, X.W., 2002. Osteoblast differentiation influences androgen and estrogen receptor-alpha and -beta expression. J. Endocrinol. 175, 683–694.

Wiren, K.M., Toombs, A.R., Semirale, A.A., Zhang, X., 2006. Osteoblast and osteocyte apoptosis associated with androgen action in bone: requirement of increased Bax/Bcl-2 ratio. Bone 38, 637–651.

Xu, J., Liao, K., 2004. Protein kinase B/AKT 1 plays a pivotal role in insulin-like growth factor-1 receptor signaling induced 3T3-L1 adipocyte differentiation. J. Biol. Chem. 279, 35914–35922.

Xu, S., Cwyfan-Hughes, S.C., van der Stappen, J.W., Sansom, J., Burton, J.L., Donnelly, M., Holly, J.M., 1996. Altered insulin-like growth factor-II (IGF-II) level and IGF-binding protein-3 (IGFBP-3) protease activity in interstitial fluid taken from the skin lesion of psoriasis. J. Investig. Dermatol. 106, 109–112.

Xu, Q., Lin, H.Y., Yeh, S.D., Yu, I.C., Wang, R.S., Chen, Y.T., Zhang, C., Altuwaijri, S., Chen, L.M., Chuang, K.H., et al., 2007. Infertility with defective spermatogenesis and steroidogenesis in male mice lacking androgen receptor in Leydig cells. Endocrine 32, 96–106.

Yeh, S., Tsai, M.Y., Xu, Q., Mu, X.M., Lardy, H., Huang, K.E., Lin, H., Yeh, S.D., Altuwaijri, S., Zhou, X., et al., 2002. Generation and characterization of androgen receptor knockout (ARKO) mice: an in vivo model for the study of androgen functions in selective tissues. Proc. Natl. Acad. Sci. U. S. A. 99, 13498–13503.

Yi, K.W., Shin, J.H., Seo, H.S., Lee, J.K., Oh, M.J., Kim, T., Saw, H.S., Kim, S.H., Hur, J.Y., 2008. Role of estrogen receptor-alpha and -beta in regulating leptin expression in 3T3-L1 adipocytes. Obesity (Silver Spring) 16, 2393–2399.

Yu, I.C., Lin, H.Y., Liu, N.C., Wang, R.S., Sparks, J.D., Yeh, S., Chang, C., 2008. Hyperleptinemia without obesity in male mice lacking androgen receptor in adipose tissue. Endocrinology 149, 2361–2368.

Zhang, Y., Calvo, E., Martel, C., Luu-The, V., Labrie, F., Tchernof, A., 2008. Response of the adipose tissue transcriptome to dihydrotestosterone in mice. Physiol. Genomics 35, 254–261.

Zhang, H.H., Huang, J., Duvel, K., Boback, B., Wu, S., Squillace, R.M., Wu, C.L., Manning, B.D., 2009. Insulin stimulates adipogenesis through the Akt–TSC2–mTORC1 pathway. PLoS One 4, e6189.